

SLAC-PUB-5096
LBL 27800
October 1989
(A)

STUDY OF MODIFIED SEXTUPOLES FOR DYNAMIC APERTURE IMPROVEMENT IN SYNCHROTRON RADIATION SOURCES*

M. CORNACCHIA
*Stanford Linear Accelerator Center
Stanford University, Stanford, CA 94309*

and

K. HALBACH
Lawrence Berkeley Laboratory, Berkeley, CA 94720

Abstract

The possibility of increasing the dynamic aperture in high brilliance synchrotron radiation sources by shaping the field of the chromaticity correction sextupoles is discussed. A new type of chromaticity correction magnets ("modified sextupoles") is proposed, having the property of behaving like sextupoles near the magnetic axis, and more linearly at larger distances. It is shown that a large increase of dynamic aperture is achievable with this method. The off-momentum behavior is discussed in terms of chromatic properties and dynamic aperture. Several types of field shape are considered. The technique for designing such magnets is presented, together with an example of magnets that give the required field distribution.

The proposed modified sextupoles seem particularly suitable for application to very small emittance synchrotron radiation sources and/or damping rings, where the strong focusing requirements often lead to insufficient dynamic aperture.

Submitted to Nuclear Instruments and Methods A.

* Work supported by Department of Energy contract DE-AC03-76SF00515.

1. Introduction

Achieving a large dynamic aperture represents one of the most challenging aspects of third- and future-generation synchrotron radiation sources. The requirements of small emittance, necessary in order to exploit the full potential of long undulators and to achieve near diffraction limited conditions, affects the design of the lattice and the electron beam dynamics. A small emittance is achieved by reducing the dispersion and the horizontal beta functions in the dipoles. This is obtained with strong focusing optics that have the disadvantage of requiring strong chromaticity correction sextupoles. The nonlinear and chromatic effects of the sextupole manifest themselves at large betatron and momentum amplitudes, compromising (if not corrected) the operation of the machine. A small dynamic aperture negatively affects the injection process and may reduce the beam lifetime via gas and Touschek scatterings. Of the above, the injection process is the most critical. In the rest of this report, we will assume that injection takes place in the horizontal plane.

The linearity of the lattice can be increased by adding several families of sextupoles beside the two required for chromaticity correction. Additional sextupole families have the strength and periodicity such as to cancel the driving terms of the resonances excited by the chromaticity sextupoles. This method has been successfully applied to several machines with excellent results. As the strength of the sextupoles increases with stronger and stronger focusing lattices, however, even this method shows its limitations. The sextupolar compensation is very sensitive to the optical transfer functions between sextupoles: in the new generation of light sources, the sextupole periodicity is broken by the presence of insertion devices and the effect of random quadrupole errors. This is particularly true for the UV and soft x-ray sources in the electron beam energy range of 1-2 GeV.

In the next section we examine the possibility of turning the strong focusing characteristics of high-brilliance synchrotron radiation sources into an advantage for increasing the dynamic aperture limit, particularly in the horizontal plane, where (we assume) injection takes place.

In sec. 2 we discuss the chromaticity correction magnet requirements. We show how, by appropriately shaping the field of these magnets (that we will call from now on “modified sextupoles”), the dynamic aperture can be increased. The effect of a modified sextupole on the dynamics of the off-momentum particle is also discussed.

In sec. 3 we describe a technique for the design of modified sextupoles and provide examples of magnets that give the required field distribution.

For the sake of example we will apply our considerations to a “triple bend achromat-lattice” of the types adopted by the Advanced Light Source (ALS) at Lawrence Berkeley Laboratory [1] and the Synchrotron Radiation Research Center at Taipei [2]. The intention of this paper is not, however, to focus on any particular machine, but to report on the general points we perceive as being important for the understanding of the particle dynamics and of the design of a new type of magnets.

The initial results of the study are encouraging. More work is needed on the outstanding issues, as reported in sec. 2.5.

2. Chromaticity correction and dynamic aperture

2.1 Chromaticity sextupole requirements

Chromaticity sextupoles are required to accomplish two tasks: to correct the chromaticity to avoid the head-tail instability and to reduce the momentum-dependent tune spread.

In order to avoid growth of the head-tail instability the chromaticity must be nonnegative where the bunch charge density is appreciable. A few standard deviations away from the center of the bunch in the two transverse directions, the chromaticity is allowed to be different from zero (and usually is, due to chromatic aberrations). The tune spread at the tail of the momentum distribution must be kept reasonably small in order to be contained within the available tune space in the working diagram. The most severe demand on the momentum-dependent tune spread in the tail of the charge distributions comes from the quantum emission of light and from the Touschek effect. The latter is particularly important for high-brilliance synchrotron radiation sources in the 1–2 GeV energy range, where a momentum acceptance of $\pm 2\%$ or more is required (equivalent to 20 or more standard deviations for a typical 1–2 GeV machine).

In summary, the chromaticity sextupoles fulfill the need of correcting the chromaticity to zero at the core of the beam and of limiting the momentum-dependent tune shifts at large momentum deviations.

2.2 Aperture requirements

Because of the strong focusing characteristics of third-generation light sources, the dispersion function is generally small at the sextupole location. Table 1 gives the values of the dispersion at the sextupoles in the ALS, together with the transverse dimensions of the beam for momentum deviations corresponding to three standard deviations, 3σ (head-tail instability region), and to the height of the RF bucket ($\pm 3\%$, as required by Touschek lifetime considerations). Momentum deviations and associated beam sizes refer to one side of the momentum distribution (+ or –). SF and SD denote the locations of the horizontal and vertical chromaticity correction sextupoles.

Table 1

Transverse beam half-size at the sextupole location due to its momentum spread.

	SF	SD
Dispersion (m)	0.21	0.14
Core of the beam:		
Relative momentum ^{a)} spread (3σ)	0.004	0.004
Momentum beam size (mm)	0.84	0.56
Tail of the beam:		
Relative momentum spread	0.030	0.030
Momentum beam size (mm)	6.3	4.2

^{a)} Typical value; the actual value depends on the charge per bunch and the RF voltage (see ref. [1]).

Next we consider the betatron motion. The maximum amplitude of the betatron oscillations is determined in the horizontal plane by the injection process and by Touschek and gas scattering. In the vertical plane the gap of the insertion devices often determines the maximum allowable amplitude of the vertical oscillations.

The nonlinear correction in the horizontal plane is required to be a sextupole field of up to 0.84 and 0.56 mm, respectively, in the SF and SD magnets. Up to a distance of 6.3 and 4.2 mm the nonlinear correction must be such as to limit the momentum-dependent tune shift. The rest of the useful aperture must simply provide a stable region for the betatron oscillations. Injection typically requires a stable region of the order of 10–15 mm. There is no requirement for the magnetic field in this region to strictly follow a quadratic dependence on amplitude.

We suggest, therefore, that the field in the sextupole magnets could be shaped, above a given distance from the magnetic axis, in such a way as to provide a more linear motion for betatron oscillations of large amplitudes. This approach has the potential to provide a wider dynamic aperture.

In the next section we analyze possible analytical expressions for the magnetic field, compute the dynamic aperture and chromatic properties, and compare them with the ones obtained with conventional sextupoles.

2.3 Example of modified chromaticity sextupoles and associated dynamic aperture

In what follows we will use the complex notation for the magnetic field $B^* = B^*(z)$, where $z = x + iy$ [see eq. (6) in sec. 3].

Consider now the following field shape:

$$B^* = -iS z^2 e^{Kz^2} \quad , \quad (1)$$

where $i^2 = -1$; S and K are constants. In this paper we will refer to this field as a ‘‘Gaussian sextupole.’’ The coefficient K in the exponential of eq. (1) is called the ‘‘damping coefficient.’’

The horizontal and vertical field components are:

$$B_y = S \exp[K(x^2 - y^2)] [(x^2 - y^2) \cos(2Kxy) - 2xy \sin(2Kxy)] \quad , \quad (2)$$

$$B_x = S \exp[K(x^2 - y^2)] [(x^2 - y^2) \sin(2Kxy) + 2xy \cos(2Kxy)] \quad . \quad (3)$$

The constant S must be chosen so as to satisfy the conditions of chromatic correction in the momentum aperture discussed above. The constant K modifies the strength of the magnetic field at large betatron amplitudes compared to a purely sextupolar field. The form of the term $\exp[K(x^2 - y^2)]$ indicates that if the horizontal bending field decreases at large horizontal amplitudes, it increases at large vertical amplitudes and vice-versa. We tried to exploit the strong focusing aspect of the accelerator and chose opposite signs for the K constant in the F and D sextupoles: the F -sextupole

acts mostly in the horizontal plane (the horizontal β -function value is 3.6 m at the SF location and that of the vertical β -function is 1.9 m), and in this plane the field must be “damped” at high amplitudes (negative sign of the damping coefficient K_F). In the D -sextupoles, on the contrary, the vertical betatron amplitudes are larger than the horizontal (horizontal β -function value: 1.5 m; vertical β -function: 9.2 m), and the damping coefficient K_D is given a positive sign.

The heart of the problem consists in selecting a pair of values for the coefficients K_F and K_D in the horizontal and vertical chromaticity correcting magnets that increase the dynamic aperture at large betatron amplitudes while preserving, as much as possible, good chromatic properties within the momentum spread of the beam. These conditions are evidently conflicting, as any departure from a pure sextupole field is bound to increase the variation of tune with momentum.

We have considered various sets of values for the constant K . Consider, for example, the value $K_F = -1000 \text{ m}^{-2}$ for the horizontal chromaticity correction magnets. Figure 1 shows the horizontal deflecting field in the horizontal plane ($y = 0$) as a function of the distance from the magnet axis. The field is compared with the one given by a pure sextupole field.

The lattice used for our study was the ALS lattice (fig. 2). The codes GEMINI/FUTAGO were used for the tracking studies.^{b)} A simplified tracking code, written in Basic for a Macintosh personal computer, was also used for quick checks. This simple code gives results largely in agreement with the sophisticated GEMINI/FUTAGO codes. In most cases, a particle is tracked 400 or 800 turns, depending on the ambiguity of the results.

b) The codes GEMINI/FUTAGO (ref. [3]) have been appropriately modified by their authors (H. Nishimura and E. Forest) to allow the possibility of including unconventional magnets in the lattice, such as the ones used in this report.

Because of the complexity of the beam dynamics issues involved, we discuss the results separately for different assumptions. These are:

- Horizontal plane motion only, on-momentum particle.
- Coupled motion horizontal-vertical plane, on-momentum particle.
- Effect of lattice magnet errors.
- Variation of tune with momentum deviation.
- Dynamic aperture for off-momentum particle, no synchrotron motion.

2.3.1 *Horizontal plane motion only (no coupling)*

(on-momentum particle, no magnetic errors)

If a particle is launched in the horizontal plane with no initial vertical coordinates, it will stay in this plane if the magnetic fields are of the “normal” type (nonskew). In this case it is easy to increase the dynamic aperture with a suitable choice of the “damping coefficient” K introduced in eq. (1). As an example, consider replacing the normal horizontal correcting sextupole of the ALS with a Gaussian sextupole having a damping coefficient $K_F = -1000 \text{ m}^{-2}$. The vertical correcting chromaticity magnet is also a Gaussian sextupole with the damping coefficient of the opposite sign: $K_D = 1120 \text{ m}^{-2}$. The coefficient K_D of this magnet has the wrong sign for the motion in the horizontal plane, but its damaging effect in the horizontal plane is reduced because of the smaller horizontal β -function at its location. For a particle launched in the horizontal plane only, the tracking simulation gives the following results^{c)}:

c) The dynamic aperture at a given point of the accelerator is defined as follows: A test particle is launched at that point with initial conditions x, x', y, y' . These initial conditions define the amplitudes of the linear motion. The maximum initial amplitude that is stable in the presence of nonlinear perturbations is the dynamic aperture. In our studies the dynamic aperture is computed in the middle of a straight section (point C in fig. 2, where $\beta_x = 11.0 \text{ m}$ and $\beta_y = 4.0 \text{ m}$).

Horizontal dynamic aperture of the ALS with normal sextupoles:	23.1 mm
Horizontal dynamic aperture with Gaussian sextupoles:	45.0 mm

No physical aperture limit was imposed in the computations. The mathematical expression for the field extends to infinity in the simulation. In practice, for a realistic magnet (see sec. 3) the field follows the required law up to a distance of the order of 25–30 mm in the sextupoles.

A calculation of the width of the main third integer resonance, $3\nu_x = \text{integer}$, driven by a normal sextupole and a Gaussian sextupole, gives a qualitative understanding for the dynamic aperture increase. The resonance width definition is given in the Appendix. Figure 3 shows the ratio of the resonance widths for the two magnets as a function of the maximum betatron amplitude. At an amplitude of 30 mm the resonance width of a Gaussian sextupole is one-third the size of that driven by a normal sextupole. For this reason Gaussian sextupoles are more forgiving in terms of resonance overlap and amplitude-dependent tune shift. The latter is shown in fig. 4. The amplitude-dependent tune shift of fig. 4 is computed by Fourier-analyzing the tracking data.

2.3.2 Coupled motion (on-momentum particle, no magnetic errors)

When the horizontal and vertical motions are coupled, the analysis becomes more complicated. The effectiveness of the Gaussian sextupoles depends on the differences of the values of the horizontal and vertical β -functions at the sextupole locations. As mentioned earlier, and as is evident by considering the field components of eqs. (2) and (3), the damping coefficients of the F - and D -Gaussian sextupoles have opposite signs in each plane. Nonetheless, it is possible to find a set of values for the damping coefficients K_F and K_D that give an overall increase in dynamic aperture. This is

shown in fig. 5. In our search for a good solution we have placed the emphasis on the improvement in the horizontal plane, since we believe it to be more critical for injection. By increasing the strength of the damping coefficient K_D at the SD location it would be possible to improve the vertical dynamic aperture at the expense of the horizontal one. A change of emphasis from the horizontal to the vertical plane may be required, for example, in order to make the vertical motion less sensitive to the breaking of the periodicity caused by the presence of insertion devices.

2.3.3 Effect of random errors

We have tracked particles in a perturbed lattice, where the perturbations are given by random quadrupole errors in the quadrupoles. A relative quadrupole error of standard deviation $\langle \Delta g/g \rangle = 0.001$ was randomly distributed according to a Gaussian distribution truncated at ± 2 standard deviations. The main cause of dynamic aperture reduction is due to the breaking of the sextupole periodicity caused by random quadrupole errors [4]. Because of the reduced strength of the sextupole driving term at large amplitudes, it is to be expected that the dynamic aperture enlargement observed in fig. 5 will also apply to a machine with random errors. This is shown in fig. 6, where the results of tracking five machines with different sets of random errors is shown. The dynamic aperture with Gaussian sextupoles is still nearly a factor of 2 larger than that obtained with normal sextupoles.

2.3.4 Variation of tune with momentum deviation

This is the crucial problem of the Gaussian sextupoles. By definition, the field departs significantly from a pure sextupole field at some distance from the magnetic axis (fig. 1). At large momentum deviation the effectiveness of compensating for the chromaticity decreases and the variation of tune with momentum increases.

The severity of the problem depends on the values of the lattice functions at the sextupoles, and thus on the detail of the lattice: the smaller the dispersion, the less important the problem. The benefits of Gaussian sextupoles increase with the focusing of the optics. We expect that very small emittance, high-brilliance, light sources, and damping rings would benefit most from this technique of chromaticity correction.

Figure 7 shows the tracking results of tune with momentum in the ALS with normal and Gaussian sextupoles. For relative momentum deviations larger than 2%, the horizontal chromaticity correction of the Gaussian sextupoles is considerably worse than with normal sextupoles. Because the dispersion is smaller at the vertical correcting sextupoles, the vertical chromaticity correction is not any worse with Gaussian sextupoles.

It is possible to symmetrize the tune spread across the momentum aperture simply by increasing the field strength [coefficient S in eqs. (1), (2) and (3)]. This is shown in fig. 8, where the chromaticity of the on-momentum particle is now positive. The natural chromaticities ($\Delta\nu/\Delta P/P$) of the ALS are -24.1 (horizontal) and -28.5 (vertical). In fig. 8 the horizontal chromaticities of the on-momentum particle are now $+1.5$ and the vertical chromaticity is still zero. The small positive chromaticity of the on-momentum particle is still effective in fulfilling its task of avoiding the head-tail instability.

2.3.5 Dynamic aperture of the off-momentum particles

The dynamic aperture of off-momentum particles is strongly affected by the feed-down effect of the Gaussian sextupoles. An off-momentum particle is now subject to even (given by the symmetry of the lens) and odd multipoles (given by the asymmetry of the closed orbit with respect to the lens axis). The odd multipoles contribute to

the first-order amplitude-dependent tune shift (the first contributor is an octupole term). These shifts have been calculated by numerical integration of eq. (A9) in the Appendix for $m = 0$ and are shown in fig. 9.

The horizontal amplitude-dependent tune decreases with betatron amplitudes for positive momentum deviation and increases for negative momentum deviation. Since the second-order even-multipole-dependent tune shift decreases with amplitude (see fig. 4), the overall result is an asymmetric dependence of amplitude-dependent tune with momentum deviation:

- For positive momentum deviation, the first-order horizontal amplitude-dependent tune shift adds to the second-order one.
- For negative momentum deviation the first-order amplitude-dependent tune shift subtracts to the second-order one.

The total amplitude-dependent horizontal tune shift, computed by Fourier analysis of the horizontal displacement, is given in fig. 10 as a function of the betatron amplitudes for various values of the momentum deviation.

The horizontal dynamic aperture of the off-momentum particles is shown in fig. 11. In order to simulate more closely a real machine (and since the horizontal plane alone often gives a very large dynamic aperture that quickly collapses when a small vertical amplitude is added to the motion), in the simulation the particle was launched with a vertical amplitude which was 6.5% of the horizontal amplitude (in normalized Courant–Snyder coordinates). The phase-space plot unmistakably shows that the dynamic aperture depression at $\Delta P/P = -1\%$ is due to the effect of the proximity of the single isolated systematic resonance $5\nu_x = 120$. The small amplitude-dependent tune shift at this momentum deviation facilitates locking to the resonance. The dynamic aperture depression at $\Delta P/P = 1\%$ is caused by coupling resonances of high order.

The pattern of the dynamic aperture of normal sextupole magnets does not show an appreciable dependence on the momentum deviation: the amplitude-dependent tune shift varies little with momentum deviation and is never small. In this case the dynamic aperture limit is more easily attributable to the overlapping of many resonances than to the effect of a single isolated one.

2.4 Other types of modified sextupoles

So far we have discussed exclusively the sextupoles with Gaussian damping. One can design a large number of field distributions that satisfy the generic conditions of behaving like a "normal" sextupole in the vicinity of the origin, but increasing in field strength less strongly than a sextupole along the x -axis for locations where $\beta_x \gg \beta_y$ (F -sextupole), or increasing less strongly than a sextupole along the y -axis for regions where $\beta_y \gg \beta_x$. Examples of such fields are:

$$\frac{B_1^*}{i} = \sqrt{1+z^2} - 1 \quad ,$$

$$\frac{B_2^*}{i} = \frac{z^2}{\sqrt{1+z^2}} \quad ,$$

$$\frac{B_3^*}{i} = \frac{z^2}{(a + \sqrt{1+z^2})} \quad ,$$

$$\frac{B_4^*}{i} = z \tanh(z) \quad ,$$

$$\frac{B_5^*}{i} = \frac{z^2}{\cosh(z)} \quad ,$$

$$\frac{B_6^*}{i} = z^2 e^{-z^2} \quad \text{(Gaussian sextupole)} \quad ,$$

and

$$\frac{B_7^*}{i} = 1 - \cos z + \epsilon (1 - \cos(mz)) \quad \text{(cosine sextupole)} \quad .$$

Besides the Gaussian sextupole type we examined a number of the above magnets; in particular, the cosine magnet described in detail in sec. 3. Although this magnet type produces fields that are very similar to those of the Gaussian sextupole, the effect on the beam dynamics was less favorable. This is the reason why it may be important to produce field distributions that are used for the tracking studies with great precision in the real world. In particular, it appears that the gradient distribution, rather than the field, is a measure of the “goodness” of a particular magnet. The implications are that the horizontal component of the magnetic field B_x close to the horizontal axis is an important quantity.

2.5 Outstanding issues

In this paper we are content with having pointed out the potential and the problems of a new chromaticity compensation scheme. For a particular application, further investigation would be required.

Further study should include the analysis of other types of modified sextupoles, the effects of synchrotron oscillations on the beam dynamics, the effects of the closed orbit errors on the beam dynamics and on the chromatic compensation, and the effect of high-order multipolar perturbations on the dynamic aperture.

2.6 Other applications

The technique studied in this paper conceivably can be applied to higher-order multipoles. Magnetic fields with the property of behaving like octupoles close to the magnetic axis and having a more linear behavior farther away from the axis may provide a way of introducing tune spread (Landau damping) at the core of the beam without deteriorating the dynamic aperture at large amplitudes. This may raise the threshold for the transverse instabilities of high-current, low-emittance beams.

2.7 *Conclusions of the beam dynamics study*

The work carried out so far is only the beginning of a study aimed at understanding the beam dynamics implications of a new type of magnet for chromaticity corrections in low-emittance synchrotron radiation sources and damping rings. So far the following conclusions emerge from the study:

- Modified sextupoles have the effect of increasing the dynamic aperture of the on-momentum particle and making it less sensitive to breaking of the periodicity due to, for instance, quadrupole errors. Further studies are needed to assess the effect of the insertion devices. In this case the perturbing effect is vertical, and a different set of damping coefficients may be required.
- Good chromatic properties can be preserved, depending on the amplitude of the momentum-dependent beam oscillation amplitude compared to the betatron-dependent one.
- The dynamic behavior of the off-momentum particle is affected by the feed-down effect of the modified sextupoles. The possibility of preserving good dynamic aperture over the required momentum deviation depends on the details of the lattice under study.
- Other types of modified sextupoles are possible. Different beam dynamics behavior (particularly the off-momentum behavior) is to be expected for different field configurations.
- The initial results of the study are encouraging. The technique described in this paper may provide a way of achieving ultrahigh brightness lattices without the present problem of degradation of dynamic aperture. It may be applied with

good overall performance to lattices that are designed with this application in mind: very strong focusing lattices are, potentially, the main beneficiaries.

We plan to continue the study with a test high-brilliance lattice designed *ad hoc* for this application.

- Modified octupoles may be used to provide Landau damping for transverse instabilities without deteriorating the dynamic aperture.

3. Design of modified sextupole magnets

In this section, even though some properties of specific magnets will be discussed, the main purpose is to explain generically what the main choices are for the function that describes B_y along the x -axis or the y -axis, how to design such a magnet, and the difficulties that one can encounter in the design of such a magnet. Even though this discussion of the magnet design procedures and pitfalls is formulated for the design of magnets that behave like sextupoles near the coordinate origin, clearly these procedures are of very general validity and could be applied to design, for instance, magnets that behave like any multipole in the vicinity of the coordinate origin, but behave in a very different manner away from the origin. We assume that the magnetic field distribution is controlled by iron surfaces, and we further assume that iron surfaces are scalar potential surfaces, knowing that design details associated with saturation effects can be handled successfully with the same methods used for the design of other iron magnets. If a coil is close enough to the aperture that it affects the field distribution, we assume that this is also handled in the “standard” fashion. It is a consequence of these assumptions that we need to consider only $2D$ fields in a vacuum region, bounded by $\mu = \infty$ surfaces.

It is worth restating that we are dealing with a magnet that behaves like a sextupole close to the coordinate origin, and satisfies the condition $B_x = 0$ along the x -axis and along the y -axis everywhere, i.e., also in regions where the field deviates strongly from the ideal sextupole.

It should be noted that the assumptions made above were made only to simplify the description of design procedures. For instance, if one were designing a conductor-dominated magnet or a fast-pulsed magnet with the field parallel to conducting surfaces, some of the details would look different but the basic design philosophy and considerations outlined here would still be applicable.

3.1 Notation and basic relationships

As mentioned earlier, we are dealing only with $2D$ fields in vacuum, thus allowing the application of the theory of a function of a complex variable. We use the standard notation:

$$z = x + iy = r e^{i\phi} \quad , \quad (4)$$

and

$$B = B_x + iB_y = |B| e^{i\beta} \quad , \quad (5)$$

with $i^2 = -1$ and $*$ indicating the complex conjugate of a complex quantity.

Since B_x and $-B_y$ satisfy the Cauchy-Riemann conditions,

$$B^* = B_x - iB_y \quad (6)$$

is an analytical function of z , and we are dealing mostly with that function.

The field components B_x , B_y are derivable from a scalar potential V or the component A of the vector potential that is perpendicular to the x - y plane. Since A and V satisfy the Cauchy–Riemann conditions, the complex potential function,

$$F(z) = A + iV \quad , \quad (7)$$

is also an analytical function of z , and that B^* is related to F through:

$$B^* = \frac{i dF}{dz} \quad (8)$$

is easily verified. We represent the sextupole field designed into the region close to $z = 0$ by:

$$B^* = B_x - iB_y = \frac{i dF}{dz} = ib_3 z^2 \quad ; \quad (b_3 = \text{real}) \quad (9)$$

$$F = \frac{b_3 z^3}{3} \quad . \quad (10)$$

Because of the imposed symmetry condition,

$$B_x(x,0) = B_x(0,y) = 0 \quad , \quad (11)$$

a “prescribed” field distribution,

$$B_y(x,0) = -g(x) \quad , \quad (12a)$$

uniquely prescribes the field everywhere through:

$$B^* = ig(z) = \frac{i dF}{dz} \quad . \quad (12b)$$

If we want to prescribe the fields through:

$$B_y(0, y) = -f(y) \quad ; \quad (13a)$$

the field is similarly prescribed everywhere through:

$$B^* = if \left(\frac{z}{i} \right) = \frac{idF}{dz} \quad . \quad (13b)$$

From these equations it obviously follows that both functions $g(x)$ and $f(y)$ must be even functions of their arguments, as is, of course, also obvious from the basic optical requirements.

Because of the symmetry properties expressed by eqs. (12) and (13), we mostly discuss the case where the fields are described by $g(x)$.

Since $g(x)$ will be deliberately designed to give a field that is much weaker (or stronger) than $b_3 x^2$ outside the central part of the aperture, it is interesting to note what effect that has on the field away from the x -axis. This can best be explored with the help of the mean value theorem [5] that states that the value of an analytical function averaged over the circumference of a circle equals its value at the center of the circle.

Applying this to $B^*/ib_3z^2 = g(z)/b_3z^2$ yields:

$$\int_0^{2\pi} \frac{B^*(z)}{ib_3z^2} \frac{d\phi}{2\pi} = \int_0^{2\pi} \frac{g(z)}{b_3z^2} \frac{d\phi}{2\pi} = 1 \quad . \quad (14)$$

A somewhat more interesting result is obtained by applying the mean value theorem to $\ell n(B^*/ib_3z^2)$:

$$\int_0^{2\pi} \ell n \left(\frac{B^*(z)}{ib_3z^2} \right) \frac{d\phi}{2\pi} = \int_0^{2\pi} \left(\ell n \left(\frac{|B|}{b_3r^2} \right) - i \left(\beta + 2\phi + \frac{\pi}{2} \right) \right) \frac{d\phi}{2\pi} = 0 \quad .$$

From this follows:

$$\int_0^{2\pi} \frac{\beta d\phi}{2\pi} = -2.5\pi \quad ,$$

and

$$\int_0^{2\pi} \ln\left(\frac{|B|}{b_3 r^2}\right) \frac{d\phi}{2\pi} = 0 \quad ; \tag{15a}$$

or, if $b_3 r^2$ and $|B|$ are normalized in the same way:

$$\int_0^{2\pi} \ln(|B(r, \phi)|) \frac{d\phi}{2\pi} = \int_0^{2\pi} \ln(|g(r, \phi)|) \frac{d\phi}{2\pi} = \ln(|b_3| r^2) \quad . \tag{15b}$$

While eq. (14) gives useful information, eq. (15b) gives deeper insight, since it deals with the absolute value of the magnetic field. Equation (15b) clearly expresses quantitatively the qualitatively obvious fact that if $|B|$ is smaller than the sextupole field strength in one location (on the x -axis), it has to be larger than the sextupole field strength someplace else.

3.2 Discussion of some types of field function $g(z)$

In this section we want to describe the properties of some representative functions that one might want to use to give along the x -axis a field that behaves like x^2 for small x , growing more slowly than x^2 for larger values of x .

What is described here also applies to the design of functions $f(y)$ that have the equivalent behavior, but with some minor variations that may be quite important from a practical point of view. Since vacuum chambers are usually larger in the x -direction than in the y -direction, locations of singularities (see below) that are acceptable in one case may not be acceptable in the other, and the physical nature of

the singularities exchange roles (charge filament-like singularities on the y -axis versus current filament-like singularities on the x -axis).

In the following $z = x + iy$ multiplied by an appropriate inverse scaling length.

$$g_1(z) = \sqrt{1 + z^2} - 1 \quad .$$

This function clearly behaves like $z^2/2$ for $|z| \ll 1$, and like z for $|z^2| \gg 1$. The transition region where the function changes from one behavior to the other is fairly large. Clearly $g_1(z)$ has branch points at $z = \pm i$, values that do not satisfy the condition $|z^2| \gg 1$. These branch points cannot be located in the vacuum region (the field must obviously be uniquely determined by $x + iy$).

If the branch points were excluded from the vacuum field region by using an iron pole that has the branch point coordinates inside it, such a magnet could be built, but it will not frequently be an attractive option unless one is dealing with a system that requires a vacuum chamber that has a very large aspect ratio.

$$g_2(z) = \frac{z^2}{\sqrt{1 + z^2}} \quad .$$

For $y = 0$, this function has a behavior similar to $g_1(x)$. It also has a branch point, but with $1/g_2(z) = 0$ at the branch points.

$$\begin{aligned} g_3(z) &= \frac{z^2}{a + \sqrt{1 + z^2}} \quad , \\ &= \frac{z^2 (a - \sqrt{1 + z^2})}{a^2 - 1 - z^2} \quad . \end{aligned}$$

Again, $g_3(x)$ looks similar to $g_1(x)$, but it has branch points at $z = \pm i$ and has singularities at $z = \pm \sqrt{a^2 - 1}$.

$$g_4(z) = z \tanh(z) \quad .$$

This function goes from $g_4(x) = x^2$ behavior to $g_4(x) = x$ behavior, but the transition region is very short and—for moderately large values of x —the difference $x - g_4(x)$ decreases exponentially ($\sim e^{-2x}$). While that behavior is very desirable, $g_4(z)$ has singularities at $z = \pm i\pi/2; \pm i3\pi/2; \pm i5\pi/2 \dots$ making this function unsuitable for at least some environments.

$$g_5(z) = \frac{z^2}{\cosh(z)} \quad .$$

$g_5(x)$ reaches a maximum value at $x = 2.07$ and decreases beyond that point. $g_5(z)$ has singularities at the same locations as $g_4(z)$.

$$g_6(z) = z^2 e^{-z^2} \quad .$$

$g_6(x)$ behaves similarly to $g_5(x)$, with the maximum occurring at $x = 1$. In contrast to all the functions discussed so far, it has no singularities of any kind for finite $|z|$. The drawback associated with $g_6(z)$ is the fact that the rapid decrease of $g_6(x)$ for large x is associated with an enormous increase of $g_6(z)$ along the y -axis.

$$g_7(z) = 1 - \cos z + \epsilon (1 - \cos(mz)) \quad .$$

Like $g_6(z)$, this function also has no singularities for finite $|z|$. $g_7(z)$ is not nearly as “violent” as $g_6(z)$. For $m = 3$ and for $0.2\pi < x < 0.8\pi$, $g_7(x)$ is approximately a linear function of x , a behavior that is probably desirable for the particle trajectories. There is a “hidden” problem associated with $g_7(z)$ that will be discussed in more detail below.

It should be pointed out that the customary procedure to characterize a magnet by the harmonics it produces is not practical for the magnets discussed here because one simply has to list so many harmonic strengths that the physical meaning is not apparent anymore. It is also worth noting that, at least in principle, some of these magnets may not be characterizable by harmonics. This would be the case if the largest value of x where particles "see" the field is larger than the distance from the origin to the closest singularity on the y -axis.

3.3 General magnet design procedure

In our opinion the best procedure to design an "exotic" magnet is to subject the geometry of the field shaping and producing entities (potential surfaces, coils) to a conformal transformation such that the task of designing a magnet that produces a nonuniform field is turned into the task of designing the simplest of all magnets, a dipole magnet. This has the advantage that one can use all the knowledge about dipole design, such as "recipes" about necessary pole width beyond the aperture limits to achieve a desired field uniformity, shimming of the pole, proper positioning of the coils, etc. In fact one of the frequently used magnet-computer programs (POISSON) allows analysis and design of magnets in dipole geometry even if one uses nonlinear iron [6].

Knowing what fields B^* we want to produce implies, through eqs. (12b) or (13b), knowledge of the complex potential $F(z)$ that describes potential surfaces and location of currents or charges in x - y geometry. It should be noted that the formulae for $F(z)$ of some of the field functions discussed above (e.g., g_5 , g_6) are not explicitly expressible in terms of elementary transcendental functions.

If one applies a conformal map $z(w)$ to the field shaping geometry, the complex potential in the w geometry becomes $F(z(w))$. Knowing that the magnet with the ideally wanted field distribution is to be transformed into an ideal dipole (for which the complex potential is constant $\cdot w$), we obtain the equation for the desired conformal map:

$$F(z) = \frac{w}{a} = \frac{u + iv}{a} , \quad (a = \text{constant}) ; \quad (16a)$$

$$\frac{dw}{dz} = w' = \frac{adF}{dz} = a g(z) . \quad (16b)$$

From this follows, for the relationship between the fields in z and w geometry, B_z^* and B_w^* :

$$B_w^* = \frac{idF}{dw} = \frac{idF}{dz} \frac{dz}{dw} = \frac{B_z^*}{w'} ,$$

$$B_z^* = B_w^* w' . \quad (17)$$

It should be noted that while B_z^* and B_w^* describe the actual fields for the real geometry of the magnet, w' characterizes the chosen conformal map (i.e., depends only on the desired fields, but not at all on the actual fields produced by the real pole and coil configuration). Since eq. (17) holds also for field errors (i.e., deviations from the ideal field), it follows that:

$$\frac{\Delta B_z^*}{B_z^*} = \frac{\Delta B_w^*}{B_w^*} ; \quad \frac{\Delta B_z}{B_z} = \frac{\Delta B_w}{B_w} ; \quad (18)$$

i.e., relative field errors in the z -geometry are the same as relative errors in the w -geometry, independent of the mapping function $w(z)$.

After the mapping function $w(z)$ has been determined the design procedure consists of the following steps:

- (1) Map the outer boundary of the region that cannot be occupied by any part of the magnet from the z -plane into the w -plane. This is usually the outer boundary of the vacuum chamber; for this design exercise, we use the vacuum-chamber outlined in fig. 12. One needs to map only the region that completely characterizes the magnet to be designed. In our case, because of the demanded symmetries, this is the first quadrant of the system shown in fig. 12.
- (2) Map from the z -plane to the w -plane the boundaries of the regions within which the field errors have to be smaller than predetermined values.
- (3) Design the dipole magnet in the w -plane by placing flat poles of sufficient width outside the map of the vacuum chamber, apply shims if necessary, etc. In general we design only that part of the magnet in dipole geometry that has a significant effect on the dipole field uniformity, then map that back into z -geometry, and design the rest of the magnet in z -geometry. To arrive at a really “buildable” magnet, it is often necessary to iterate a few times between the magnet representations in the z -plane and w -plane.

3.4 *Design of specific magnets*

Figure 12 shows schematically the cross section of a vacuum chamber with two inscribed good field regions to indicate crudely the core region and outer limits of the halo of the beam. We describe the design of two types of magnets. The first magnet is the sextupole with Gaussian damping (g_6 in sec. 3.2), since that is the magnet whose beam dynamics implications we have studied most. That description is followed by the magnet characterized by g_7 in sec. 3.2 (for $m = 3$). A significant amount of work was expended on this magnet; and even though the benefits obtained from this magnet are not as significant as those obtained from the sextupole with Gaussian

damping, we describe its design here because the study of this magnet yielded two interesting insights that were not clearly anticipated:

- (1) Since B_y on the coordinate axes produced by magnets characterized by $g_6(z)$ and $g_7(z)$ are nearly identical when the free constants are chosen appropriately, the fact that their optical performance is noticeably different indicates that the values of B_x near the axes (being proportional to the more noticeably different derivatives of B_y) are quite important. This difference in performance leads to the conclusion that in order to achieve the desired increase in dynamic aperture, one should try to achieve the theoretical fields with great accuracy, at least until we better understand the more subtle aspects of the optics.
- (2) While the design of the Gaussian-damped sextupole is straightforward, for not unreasonable values of the free parameters of a magnet with fields described by $g_7(z)$, it may be very difficult, or even impossible, to build a magnet that produces the desired fields within the given vacuum chamber. Since this design difficulty is due to a generic problem that can arise with some types of magnets, we choose the magnet with fields given by $g_7(z)$ as the example to demonstrate this kind of problem.

3.6 Two magnets characterized by $g(z) = z^2 e^{Kz^2}$

Figure 13 shows the map of the outer vacuum chamber wall and the two “good field” regions outlined for $K = -1000 \text{ m}^{-2}$. Since the symmetry conditions require only investigation of the magnet for $x, y > 0$ (i.e., in the first quadrant), the map of that region covers 3 quadrants, with the $x > 0$ axis mapped onto the $u > 0$ axis, and the $y > 0$ axis mapped onto the $v < 0$ axis. Figure 13 also shows the flat part of a dipole-pole in the $v > 0$ space, and one-half of such a pole in the $v < 0$ space.

The closest permitted distance of the half-pole from the v -axis is determined by the map of the vacuum chamber wall. While it is possible to have the location of the other pole equivalently determined, it is advantageous to locate that pole at the same absolute distance from the u -axis. This location insures greater symmetry, and thus quality, of the generated fields; in addition, all poles will therefore have to be excited by the same number of ampere-turns.

The shown poles are wide enough to give adequate field quality in the good field region if the ends of the poles are shimmed appropriately. We have not designed these shims here since their detailed contour depends on design details that exceed what can be described in this paper.

In order to get a qualitative indication of the local value of w' , and with it the local field strength, the maps of the vacuum chamber and the circle that forms the outer good-field region after "squashing" it into an ellipse have marker points that are equidistant in the z -plane; and the dipole-poles have markers that are equidistant in the w -plane. Figure 14 shows the maps of the dipole-poles with their markers that are shown in fig. 13. Also shown is the part of the vacuum chamber wall that falls within the figure frame given by the x and y axes and the extreme points on the poles. The location of the markers on the pole contours directly indicates the necessary width of the poles based on the understanding of the field quality achievable in the dipole geometry shown in fig. 13. For comparison fig. 14 also shows (dashed lines) the poles for the case $K = 0$, i.e., a conventional sextupole. The difference between the conventional sextupole and a modified sextupole is clearly quite pronounced.

Figures 15 and 16 correspond to figs. 13 and 14, respectively, but have been computed for $K = 1120 \text{ m}^{-2}$. Since in this magnet the field has to be smaller on the y -axis, right under a pole, than it would be for a conventional sextupole, it is

not practical to have the pole that is bisected by the y -axis on the same potential as the pole in the first quadrant. Figure 16 shows the magnet for the case in which the pole bisected by the y -axis is excited by about 10% of the excitation of the pole located in the first quadrant. It is clear without further elaboration that this magnet is extremely different from a conventional sextupole.

3.7 A magnet characterized by $g(z) = w'(z) = a [1 - \cos(kz) + \epsilon(1 - \cos(3kz))]$

One of the magnets that we investigated during the course of this study was the type of magnet with $k = 100 \text{ m}^{-2}$ and $\epsilon = -0.01$ (“cosine sextupole”). Figure 17 is the map of the vacuum chamber and the good field regions for this magnet.

Putting both poles at the same distance from the u -axis, dictated by the map of the point $x = 0, y = 23 \text{ mm}$ of the vacuum chamber, mapping them into the z -plane, and analyzing the fields with POISSON showed substantial field errors in regions where one would expect to reproduce the specified fields with great accuracy. The reason is the following:

Application of the argument principle [5] shows that for $y > 0, 0 < x < 30 \text{ mm}$, $w'(z) = 0$ at one (and only one) location. Putting an equation solver to work locates that point at $kx_1 = 1.6686; ky_1 = 2.3171$. This means that at that point the conformal map is, in fact, *not conformal*, and the map of that “danger point” is indicated in fig. 17. The consequences of the lack of conformality there are most easily understood in terms of the magnetic fields there. Since at that location $w'' \neq 0$, the field in the vicinity of that point has the properties of a quadrupole with its axes rotated by about 75° , as shown schematically in fig. 18. If one chooses pole #1 in the dipole geometry shown in fig. 17, it will map into the scalar potential surface #1 in fig. 18. While the point $z = 0$ (lacking conformality also) is surrounded by poles that

are specifically designed to make the field zero there, such poles are not present in the vicinity of the point $z_1 = x_1 + iy_1$, leading obviously to nonzero fields there. Since the fields in the vicinity of that point are not what they are supposed to be, they will be, at least to some degree, incorrect elsewhere also. In this case the problem is easily remedied by dropping the symmetry condition of having both poles excited by the same number of ampere-turns and using the pole indicated as #2 in figs. 17 and 18. The complete pole configuration for that case is shown in fig. 19, and it gives the desired field.

It is clear that when the point z_1 falls inside the vacuum chamber, the desired fields cannot be implemented. When the point z_1 is outside the vacuum chamber, but inside the frame of fig. 17, that pole could, in principle, be split into two poles, excited to different scalar potentials. But in general it will be preferable to modify some of the free parameters in such a way that the point z_1 is outside the frame in fig. 17. After all there is very great freedom in choosing the field of this modified sextupole outside the immediate core region.

Acknowledgments

The authors wish to thank Etienne Forest for the implementation in the code FUTAGO of the modifications required to track particles with magnets having the unconventional field shape discussed in this report. Thanks are also due to Hiroshi Nishimura for his help in setting up the GEMINI file. The study benefited greatly from the flexibility and the power of the tracking codes GEMINI/FUTAGO.

The authors would also like to thank Ewan Paterson for reading the manuscript and providing stimulating comments.

Appendix

In this section we derive the stop-band width and tune shift for a generalized (i.e., not necessarily expressed in multipole form) magnetic perturbation. We consider the nonlinear coupled equations:

$$\begin{aligned}\frac{d^2x}{ds^2} + K_x(s)x &= \frac{E_x(x,y,s)}{E_0} , \\ \frac{d^2y}{ds^2} + K_y(s)y &= \frac{E_y(x,y,s)}{E_0} ,\end{aligned}\tag{A1}$$

where E_0 is the particle's energy.

The Hamiltonian of the motion is of the form:

$$H = \frac{p_x^2}{2} + \frac{p_y^2}{2} + \frac{K_x(s)x^2}{2} + \frac{K_y(s)y^2}{2} + \frac{V(x,y,s)}{E_0} ,\tag{A2}$$

with $p_x = dx/ds$; $\partial V/\partial x = E_x$; and $\partial V/\partial y = E_y$.

Putting $\theta = s/R$ (R being the accelerator radius), then

$$H = \frac{p_x^2}{2} + \frac{p_y^2}{2} + \frac{R^2 K_x(\theta)x^2}{2} + \frac{R^2 K_y(\theta)y^2}{2} + \frac{R^2 V(x,y,\theta)}{E_0} .\tag{A3}$$

Transforming into action-angle variables $\phi_{x,y}$, $\zeta_{x,y}$, with

$$\begin{aligned}x &= \left(\frac{2\zeta_x\beta_x}{R}\right)^{1/2} \cos(\phi_x + \psi_x(\theta)) , \\ p_x &= -\left(\frac{2R\zeta_x}{\beta_x}\right)^{1/2} \left[\sin(\phi_x + \psi_x(\theta)) + \alpha_x \cos(\phi_x + \psi_x(\theta)) \right] ,\end{aligned}\tag{A4}$$

where

$$\psi_x(\theta) = \int_0^\theta \frac{Rd\theta}{\beta_x}$$

is the unperturbed phase and ζ is related to the "emittance" of a particle ϵ :

$$\zeta_{x,y} = \frac{\epsilon_{x,y} R}{2} .$$

The canonical variable ϕ is the perturbation to the unperturbed phase ψ . Identical expressions for the y plane are obtained by changing the subscripts.

Under this transformation the Hamiltonian becomes:

$$H = \frac{R^2}{E_0} V(\theta, \zeta_x, \phi_x, \zeta_y, \phi_y) , \quad (A5)$$

giving

$$\left. \begin{aligned} \frac{d\zeta_x}{d\theta} &= \frac{-R^2}{E_0} \frac{\partial V}{\partial \phi_x} ; & \frac{d\zeta_y}{d\theta} &= \frac{-R^2}{E_0} \frac{\partial V}{\partial \phi_y} \\ \frac{d\phi_x}{d\theta} &= \frac{R^2}{E_0} \frac{\partial V}{\partial \zeta_x} ; & \frac{d\phi_y}{d\theta} &= \frac{R^2}{E_0} \frac{\partial V}{\partial \zeta_y} \end{aligned} \right\} , \quad (A6)$$

where

$$\begin{aligned} \frac{\partial V}{\partial \phi_x} &= \frac{\partial V}{\partial x} \frac{\partial x}{\partial \phi_x} = -E_x \left(\frac{2\zeta_x \beta_x}{R} \right)^{1/2} \sin \phi_x \\ \frac{\partial V}{\partial \zeta_x} &= \frac{\partial V}{\partial x} \frac{\partial x}{\partial \zeta_x} = E_x \left(\frac{\beta_x}{2R\zeta_x} \right)^{1/2} \cos \phi_x . \end{aligned}$$

The phase equations then become:

$$\frac{d\phi_{x,y}}{d\theta} = \frac{R^2}{E_0} \left(\frac{\beta_{x,y}}{2R\zeta_{x,y}} \right)^{1/2} \cos(\phi_{x,y}) E_{x,y}(\theta, \zeta_x, \phi_x, \zeta_y, \phi_y) . \quad (A7)$$

Introducing the Fourier component of the driving term:

$$\left. \begin{aligned} G_{x,m}(\zeta_x, \phi_x, \zeta_y, \phi_y) &= \frac{1}{2\pi} \int_0^{2\pi} \beta_x^{1/2} \cos(\phi_x) E_x e^{im\theta} d\theta \\ G_{y,m}(\zeta_x, \phi_x, \zeta_y, \phi_y) &= \frac{1}{2\pi} \int_0^{2\pi} \beta_y^{1/2} \cos(\phi_y) E_y e^{im\theta} d\theta \end{aligned} \right\} , \quad (A8)$$

Equation (A7) becomes:

$$\left. \begin{aligned} \frac{d\phi_x}{d\theta} &= \frac{R^2}{E_0} \left(\frac{1}{2R\zeta_x} \right)^{1/2} \sum_m G_{x,m} e^{-im\theta} \\ \frac{d\phi_y}{d\theta} &= \frac{R^2}{E_0} \left(\frac{1}{2R\zeta_y} \right)^{1/2} \sum_m G_{y,m} e^{-im\theta} \end{aligned} \right\} . \quad (A9)$$

Introducing the slow phase:

$$\left. \begin{aligned} \tilde{\psi} &= N_x \phi_x + N_x \psi_x + N_y \phi_y + N_y \psi_y - m\theta \\ \frac{d\tilde{\psi}}{d\theta} &= N_x \frac{d\phi_x}{d\theta} + N_y \frac{d\phi_y}{d\theta} + N_x \frac{R}{\beta_x} + N_y \frac{R}{\beta_y} - m \end{aligned} \right\} . \quad (A10)$$

The resonance width of the coupled resonance $N_x\nu_x + N_y\nu_y = m$ is:

$$\Delta e = N_x \frac{\overline{d\phi_x}}{d\theta} + N_y \frac{\overline{d\phi_y}}{d\theta} ,$$

averaged over all the phases ϕ_x, ϕ_y .

We find from eqs. (A7) and (A8) retaining only the index m which gives the slow phase $\tilde{\psi}$:

$$\begin{aligned} N_x \frac{d\phi_x}{d\theta} + N_y \frac{d\phi_y}{d\theta} &= \frac{R}{E_0} \left[\frac{N_x}{\sqrt{\epsilon_x}} G_{x,m} + \frac{N_y}{\sqrt{\epsilon_y}} G_{y,m} \right] \\ &\times \exp \left\{ -i \left[N_x (\phi_x - \psi_x) + N_y (\phi_y - \psi_y) - \tilde{\psi} \right] \right\} . \end{aligned} \quad (A11)$$

Averaging over the slowly varying term $e^{i\tilde{\psi}}$, we then have

$$\begin{aligned} \Delta e &= \frac{R}{E_0(2\pi)^3} \int_{\Delta\theta_{int}} \int_0^{2\pi} \int_0^{2\pi} \left[\frac{N_x \beta_x^{1/2}}{\sqrt{\epsilon_x}} E_x \cos(\phi_x) + \frac{N_y \beta_y^{1/2}}{\sqrt{\epsilon_y}} E_y \cos(\phi_y) \right] \\ &\times \exp \{ -i [N_x (\phi_x - \psi_x) + N_y (\phi_y - \psi_y) - m\theta] \} d\phi_x d\phi_y d\theta , \end{aligned} \quad (A12)$$

where $\Delta\theta_{int}$ is the magnet length. On resonance we have $m\theta = N_x\phi_x + N_y\phi_y - N_x\psi_x - N_y\psi_y$.

Example: A pure sextupole field. Consider a single sextupole of length L :

$$E = E_x - iE_y = \bar{e}cS(x + iy)^2 = \bar{e}cS(x^2 + 2ixy - y^2) ,$$

$$E_x = \bar{e}cS(x^2 - y^2) , \quad E_y = -\bar{e}2cSxy , \quad N_x = 1 , \quad N_y = 2 ,$$

where S is the sextupole strength, c is the speed of light, and \bar{e} is the electron charge.

From eq. (A12),

$$\begin{aligned} \Delta e &= \frac{2L}{(2\pi)^3 B\rho} \int_0^{2\pi} \int_0^{2\pi} \left\{ \frac{\beta_x^{1/2} S}{\sqrt{\epsilon_x}} \cos(\phi_x) [\beta_x \epsilon_x \cos^2(\phi_x) - \beta_y \epsilon_y \cos^2(\phi_y)] \right. \\ &\quad \times \cos(\phi_x + 2\phi_y) - \frac{2\beta_y^{1/2} S}{\sqrt{\epsilon_y}} \\ &\quad \times 2 \cos(\phi_y) \sqrt{\epsilon_x \epsilon_y \beta_x \beta_y} \cos(\phi_x) \cos(\phi_y) \\ &\quad \left. \times \cos(\phi_x + 2\phi_y) \right\} d\phi_x d\phi_y , \\ &= \frac{2SL}{(2\pi)^3 \beta\rho} \int_0^{2\pi} \int_0^{2\pi} \left\{ \beta_x^{3/2} \sqrt{\epsilon_x} \cos^3(\phi_x) - \beta_x^{1/2} \beta_y \frac{\epsilon_y}{\sqrt{\epsilon_x}} \cos(\phi_x) \cos^2(\phi_y) \right. \\ &\quad \left. - 4\beta_x^{1/2} \beta_y \sqrt{\epsilon_x} \cos(\phi_x) \cos^2(\phi_y) \right\} \cos(\phi_x + 2\phi_y) d\phi_x d\phi_y . \quad (A13) \end{aligned}$$

Now

$$\int_0^{2\pi} \int_0^{2\pi} \cos^3(\phi_x) \cos(\phi_x + 2\phi_y) d\phi_x d\phi_y = 0 ,$$

and

$$\cos(\phi_x) \cos^2(\phi_y) = \frac{\cos(\phi_x)}{2} + \frac{1}{4} [\cos(\phi_x - 2\phi_y) + \cos(\phi_x + 2\phi_y)] ;$$

so retaining the coherent term,

$$\Delta e = \frac{SL}{2\pi\beta\rho} \beta_x^{1/2} \beta_y \sqrt{\epsilon_x} \left[1 + \frac{\epsilon_y}{4\epsilon_x} \right] , \quad (A14)$$

which is the well-established result for a single resonance.

Example: the Gaussian sextupole. Let's consider the Gaussian sextupole in the horizontal plane only:

$$E_x = \bar{e} c S x^2 \exp(Kx^2) . \quad (A15)$$

Integration of eq. (A12) with $N_x = 3$, $N_y = 0$ gives, for a short magnet (i.e., assuming constant lattice function values in the magnet) of length L , the resonance width of the third integer resonance driven by a single magnet:

$$\Delta e = \frac{3LS \beta_x^{3/2} \sqrt{\epsilon_x} e^{-b}}{8\pi B\rho} [I_0 - 3I_1 + 3I_2 - I_3] , \quad (A16)$$

where b is $K\beta_x\epsilon_x/2$, β_x is the horizontal beta function at modified sextupole location, ϵ_x is the invariant of linear motion ("emittance") and is equal to a^2/β_x (a being the maximum betatron amplitude in absence of nonlinear perturbation at the modified sextupole location), and I_0 , I_1 , I_2 , and I_3 are the Bessel functions of order 0, 1, 2, and 3 and argument b .

The first-order amplitude-dependent tune shift is found by numerical integration of the first equation in (A9), with $m = 0$ and by putting $x = a \cos(\phi_x)$ in eq. (A15). For an off-momentum particle the amplitude x in eq. (A15) is replaced by $x = a \cos(\phi_x) + d$, d being the orbit displacement from the on-momentum orbit.

References

1. "1-2 GeV Synchrotron Radiation Source," *Conceptual Design Report* (June 1986), Lawrence Berkeley Laboratory Report LBL-5172.
2. C. C. Kuo, J. C. Lee, S. T. Chou, C. Travier, and C. S. Hsue, "TBA6C Lattice," Synchrotron Radiation Research Center Report SRRC/BD/IM/88-15 (1988).
3. E. Forest and H. Nishimura, Lawrence Berkeley Laboratory Report LBL-25961.
4. A. Jackson, Lawrence Berkeley Laboratory Report ESG Tech-Note-103.
5. Z. Nehari, *Introduction to Complex Analysis* (Allyn & Bacon, 1968).
6. K. Halbach, *Nucl. Instr. and Meth.* **64** (1968) 278.

Figure Captions

- Fig. 1. Vertical component of the magnetic field along the horizontal axis for normal and Gaussian sextupoles with $K_F = -1000 \text{ m}^{-2}$. The vertical arrow indicates the orbit deviation for a momentum deviation of 3%, where good chromatic correction is required.
- Fig. 2. Lattice of one superperiod of the ALS. The symbol Q denotes a quadrupole magnet; B is a combined function dipole–quadrupole magnet; SF and SD are horizontal and vertical correcting chromaticity sextupoles, respectively. C is in the center of the straight section, where the dynamic aperture is computed. Picture credit: ref. 1, fig. 3.3.
- Fig. 3. Width of the third integer resonance $3\nu_x = \text{integer}$ (defined in the Appendix) driven by a single normal F -sextupole divided by the width driven by a Gaussian sextupole. The ratio is plotted as a function of the maximum betatron amplitude at the reference point (center of straight section, point C in Fig. 2).
- Fig. 4. Horizontal tune shift versus maximum betatron amplitude for normal and Gaussian sextupoles.
- Fig. 5. Dynamic aperture of on-momentum particle with normal and Gaussian sextupoles.
- Fig. 6. Dynamic aperture of five different machines having magnetic field gradient errors randomly distributed in the quadrupoles. The rms value of the distribution of the relative gradient errors is 0.001.
- Fig. 7. Horizontal and vertical tune deviations as a function of momentum deviation with normal and Gaussian sextupoles.

Fig. 8. Horizontal tune deviation versus momentum deviation with Gaussian sextupoles of positive chromaticity ($C_H = 1.5$).

Fig. 9. Amplitude-dependent horizontal tune shift driven by the first-order approximation of the Gaussian sextupoles. The tune shifts are given as a function of the maximum betatron amplitude and for two values (+1% and +3%) of the momentum deviation. Negative momentum deviation gives the same absolute value but a reverse sign to the tune shift.

Fig. 10. Total amplitude-dependent tune shifts (computed from the tracking results) at various positive and negative momentum deviations.

Fig. 11. Horizontal dynamic aperture as a function of the momentum deviation from the synchronous momentum.

Fig. 12. Vacuum chamber with good field regions.

Fig. 13. Map of vacuum chamber and good field region boundaries for Gaussian sextupole with $K = -1000 \text{ m}^{-2}$.

Fig. 14. Poles for Gaussian sextupole with $K = -1000 \text{ m}^{-2}$.

Fig. 15. Map of vacuum chamber and good field region boundary for Gaussian sextupole with $K = 1120 \text{ m}^{-2}$.

Fig. 16. Poles for Gaussian sextupole with $K = 1120 \text{ m}^{-2}$.

Fig. 17. Map of vacuum chamber and good field region boundaries for sextupole with $k = 100 \text{ m}^{-1}$ and $\epsilon = 0.01$.

Fig. 18. Scalar potential surfaces in vicinity of $w' = 0$ – point.

Fig. 19. Usable poles for sextupole with $k = 100 \text{ m}^{-1}$ and $\epsilon = 0.01$.

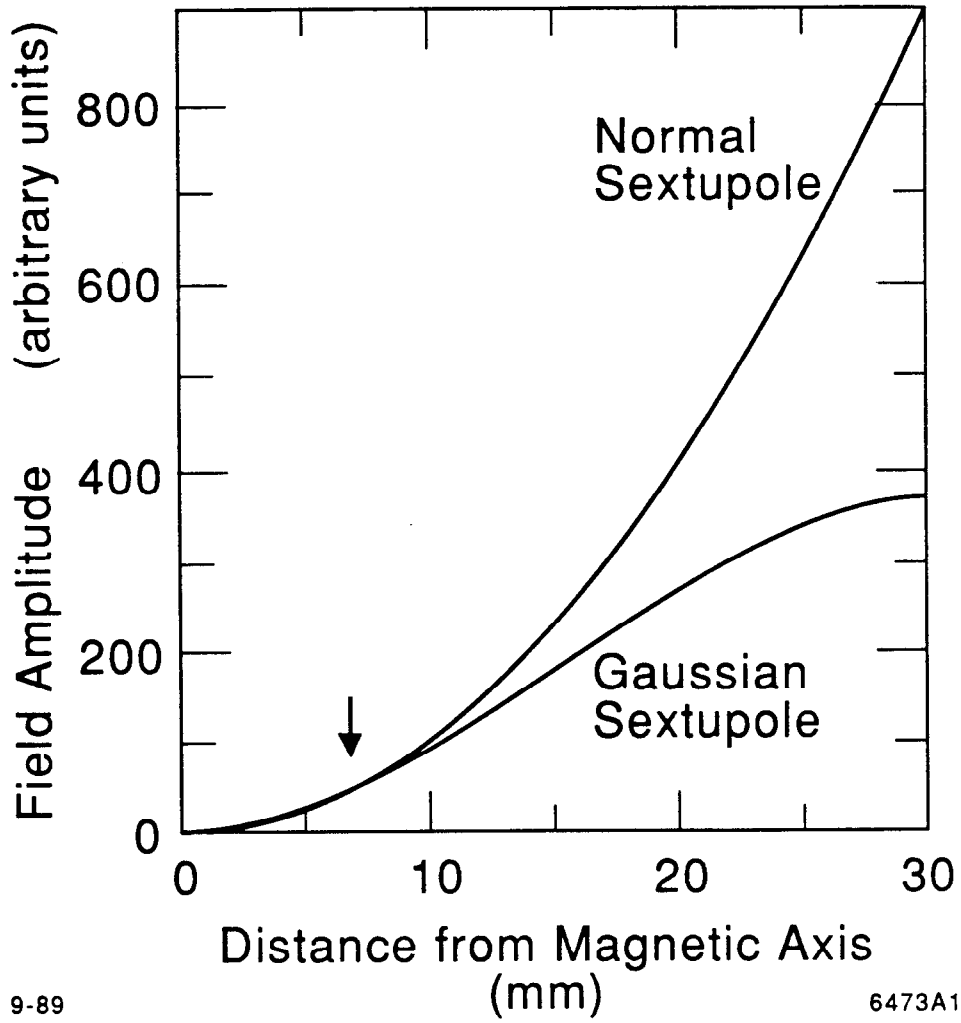
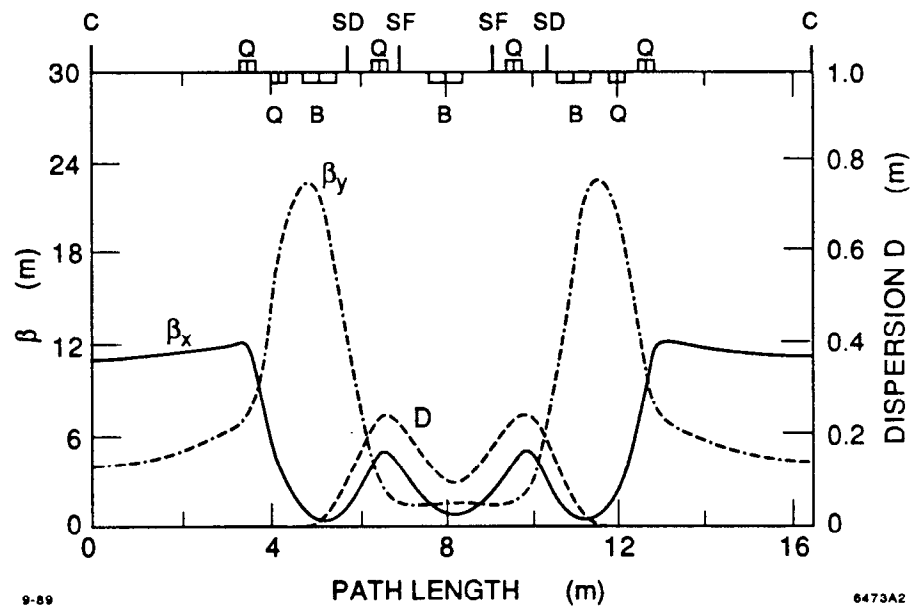


Fig. 1



9-89

6473A2

Fig. 2

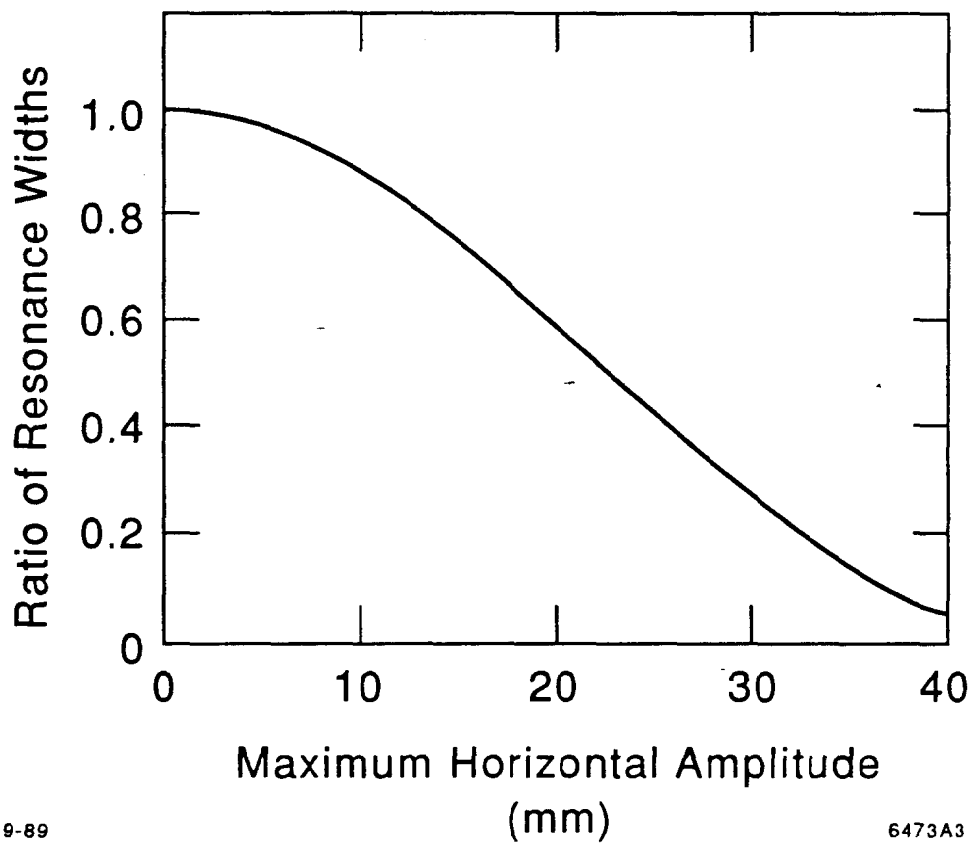
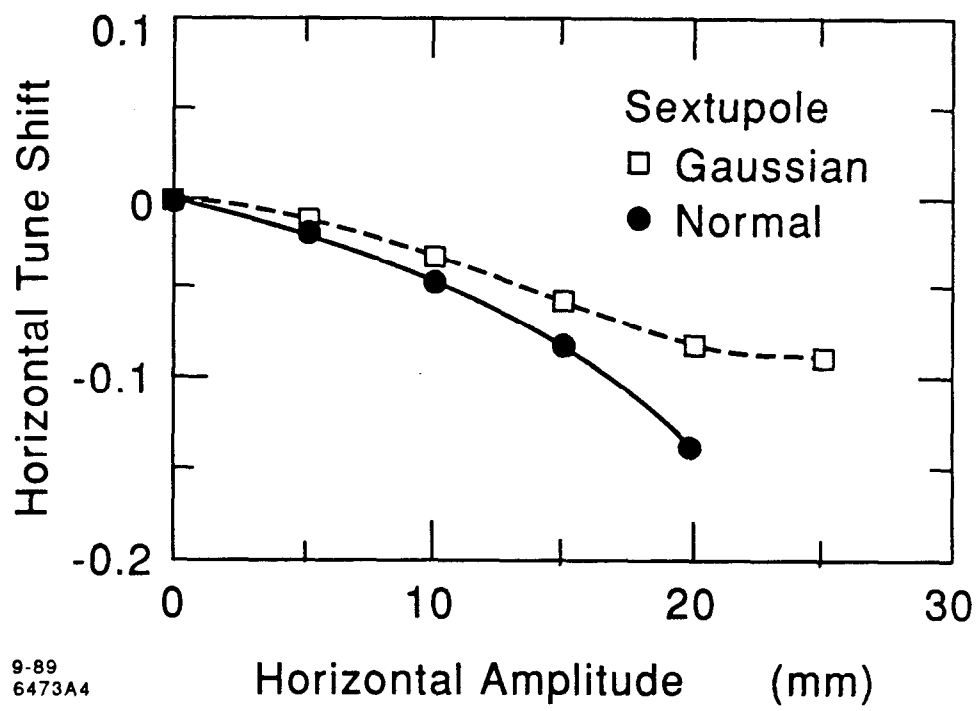


Fig. 3



9-89
6473A4

Fig. 4

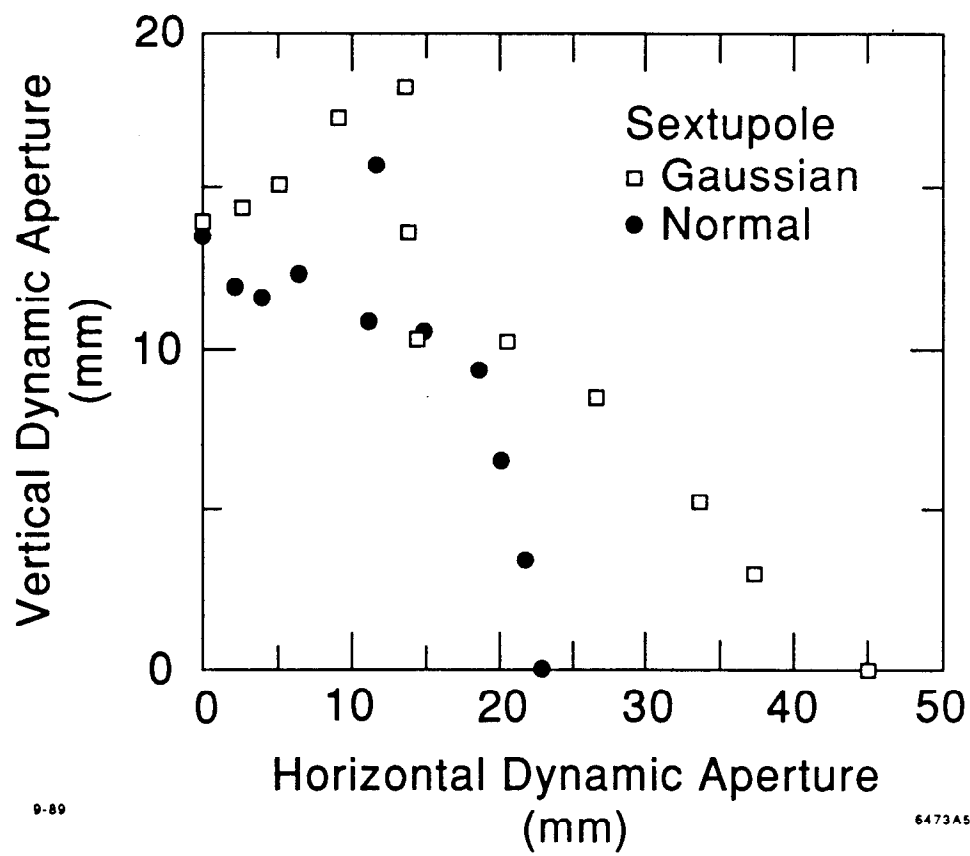


Fig. 5

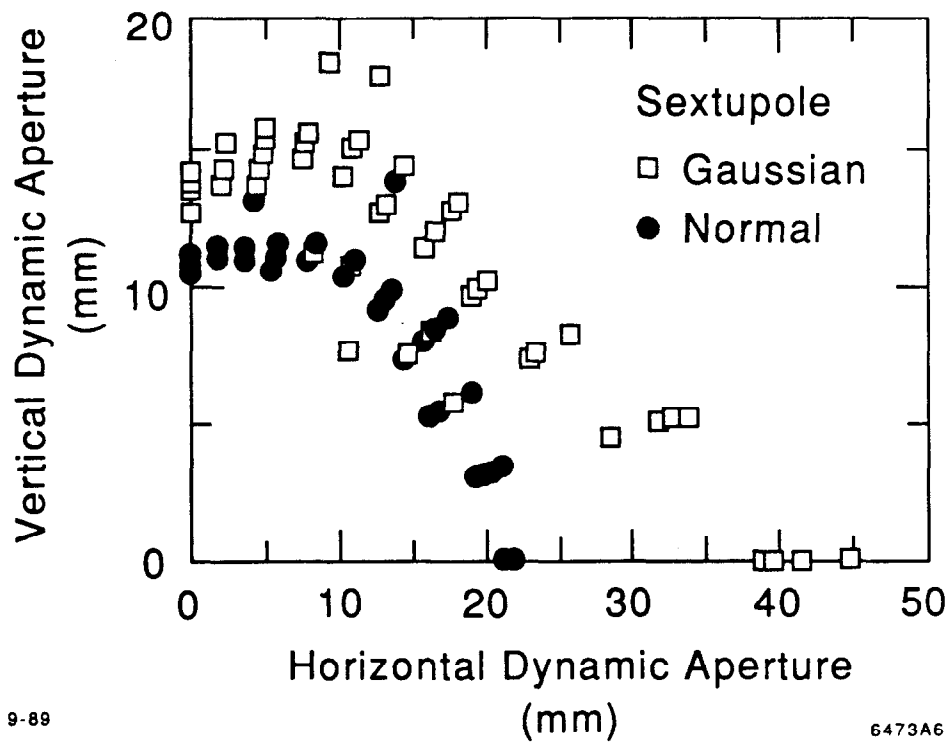
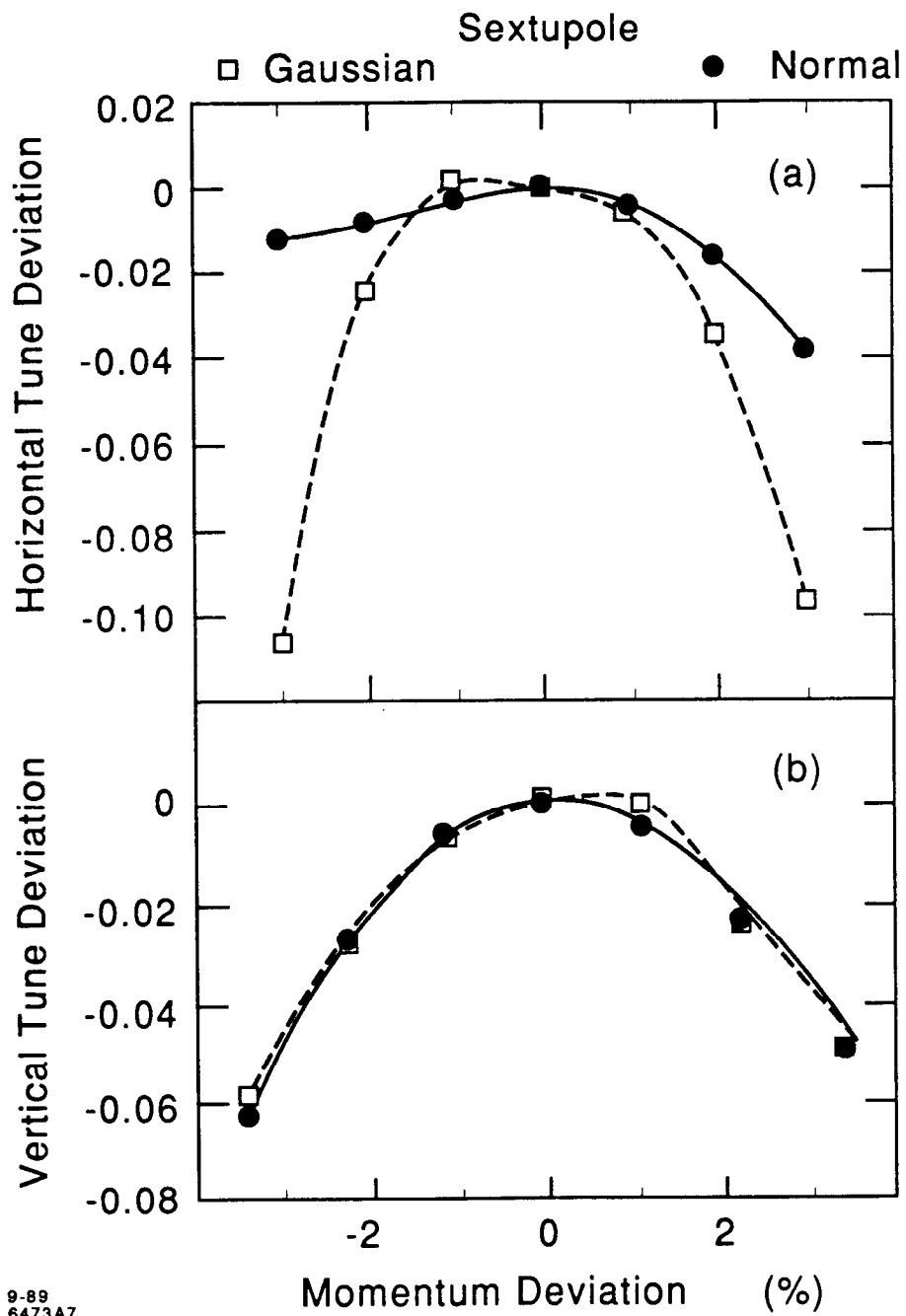
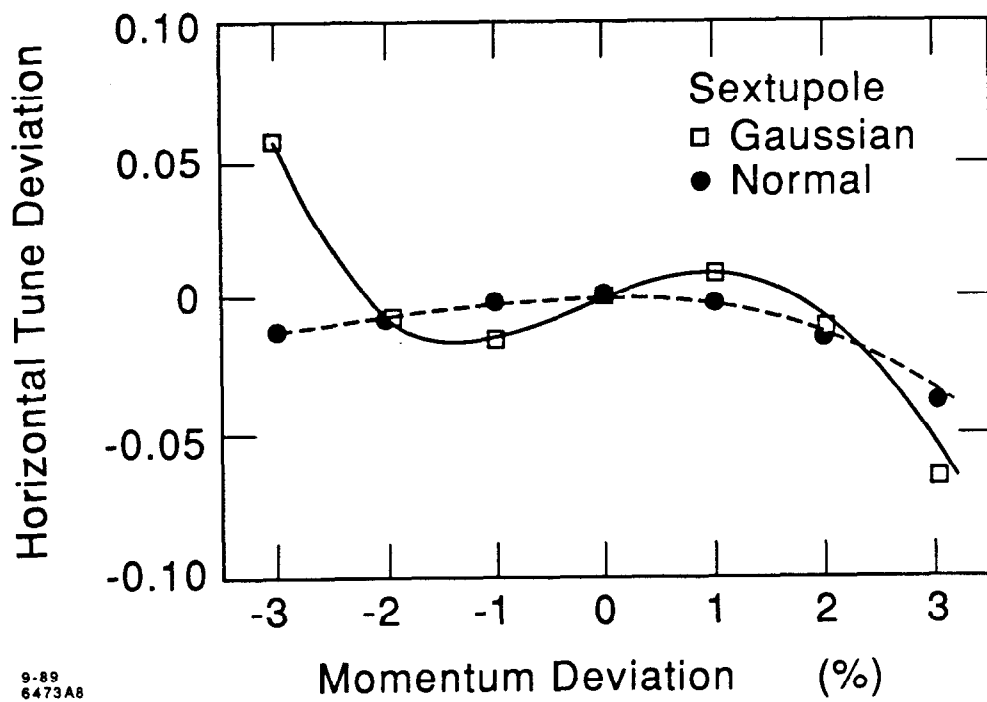


Fig. 6



9-89
6473A7

Fig. 7



9-89
6473A8

Fig. 8

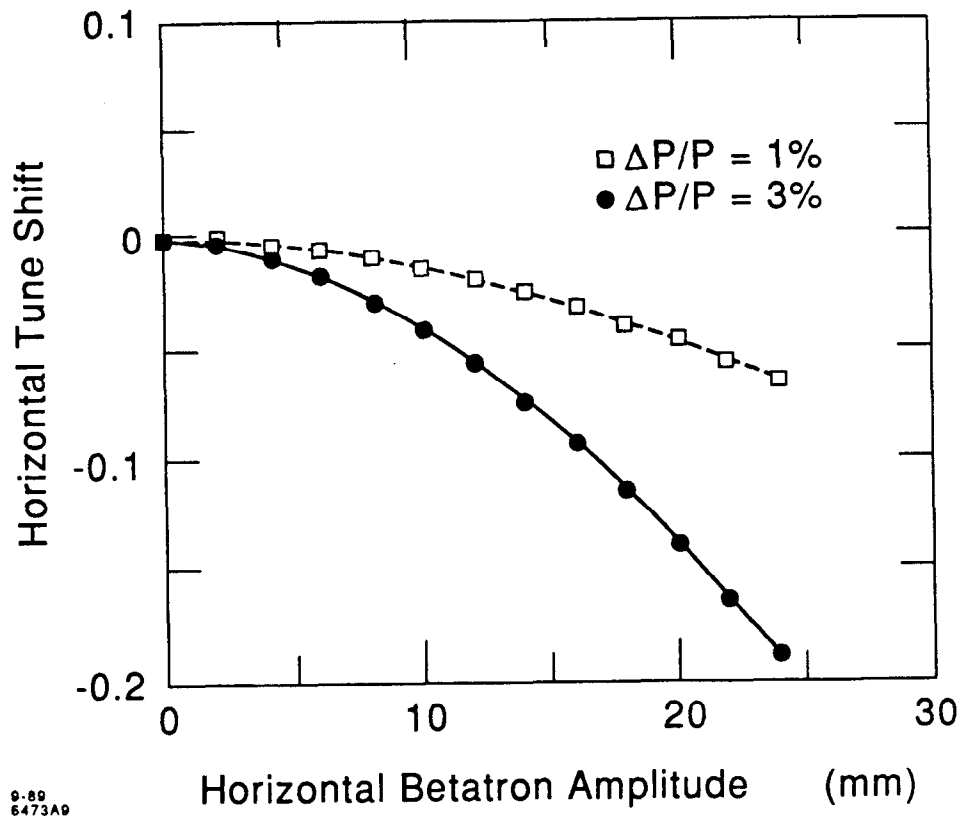


Fig. 9

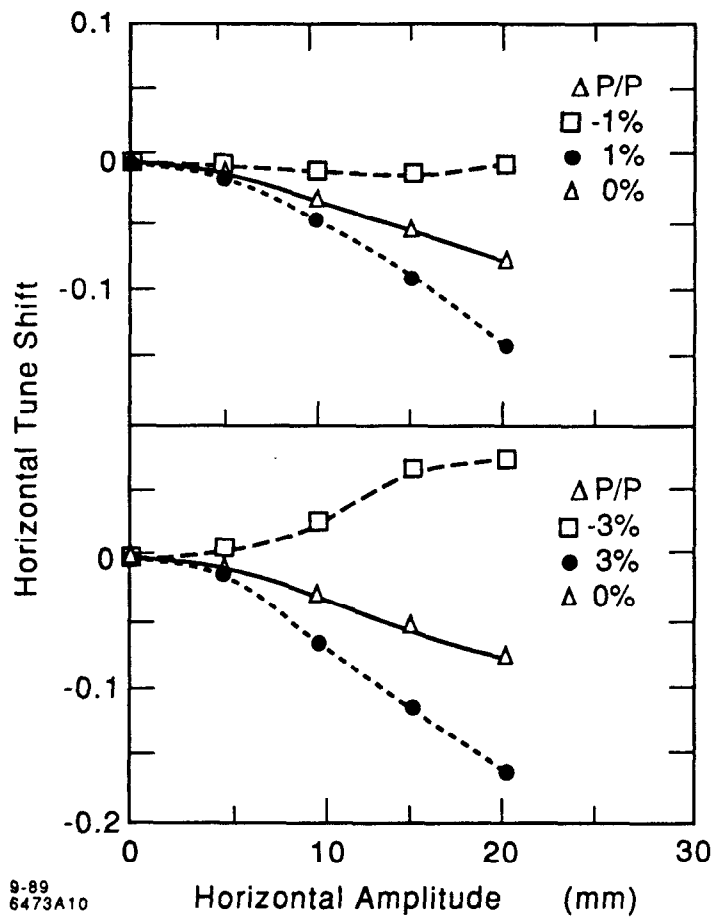


Fig. 10

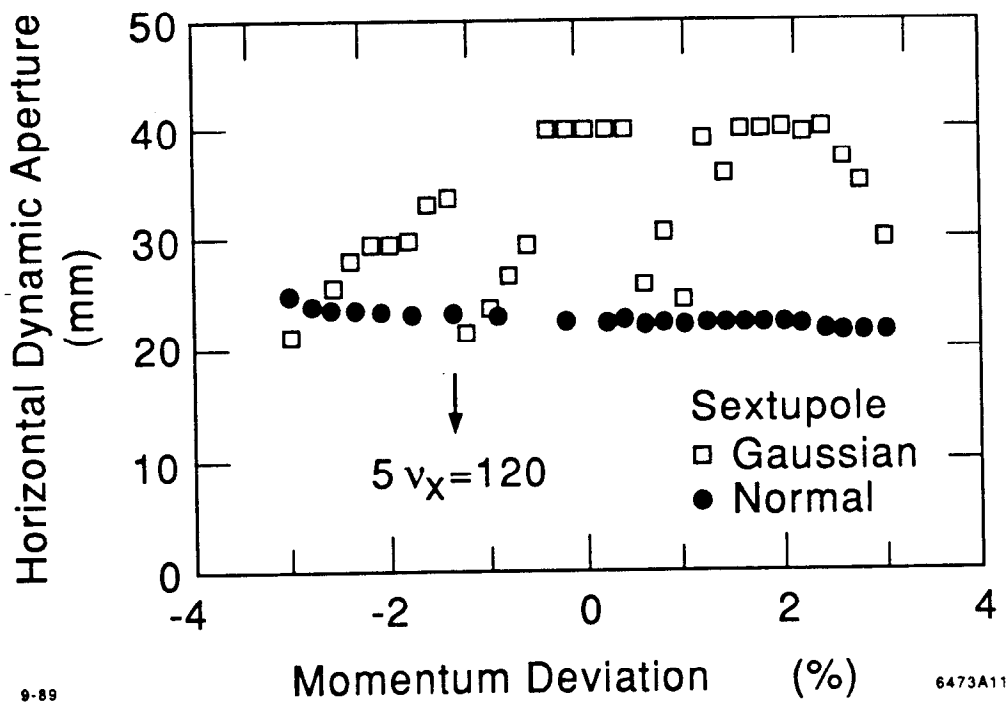


Fig. 11

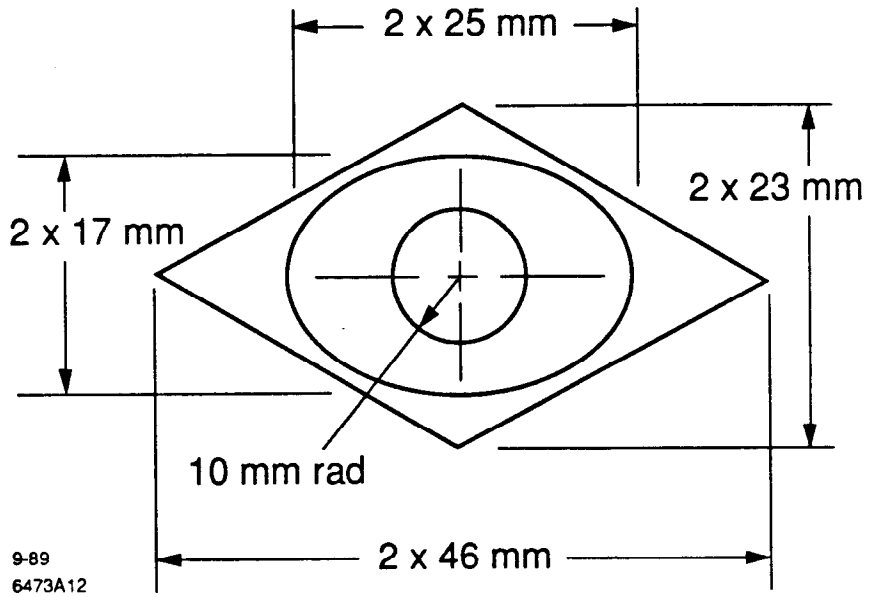
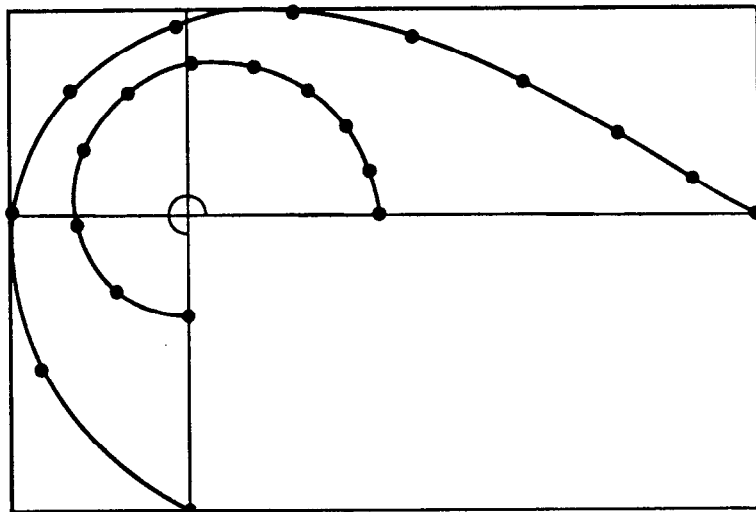


Fig. 12

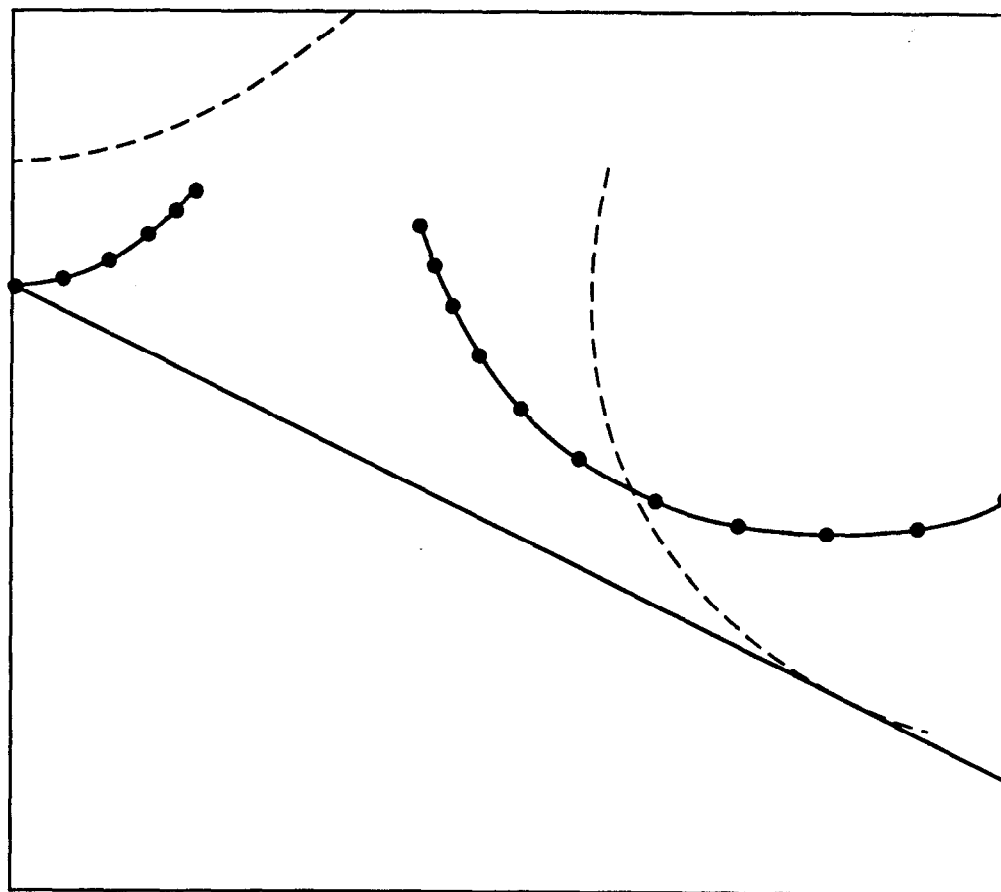


9-89

6473A13

Fig. 13

----- Poles of Conventional Sextupole
—— Poles of Modified Sextupole



9-89

6473A14

Fig. 14

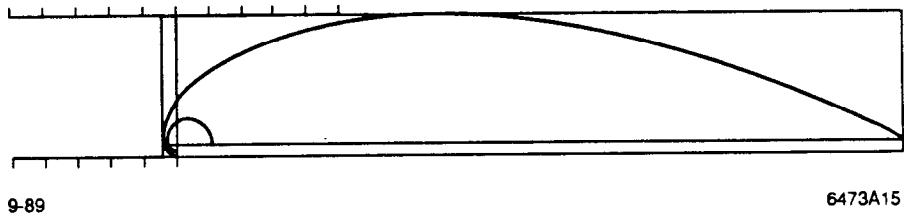
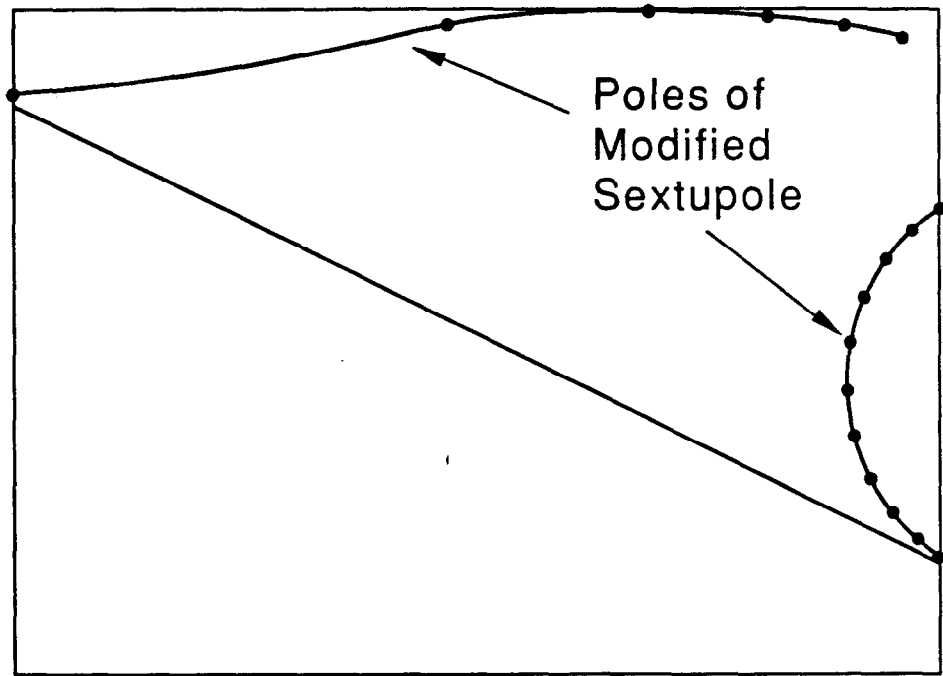


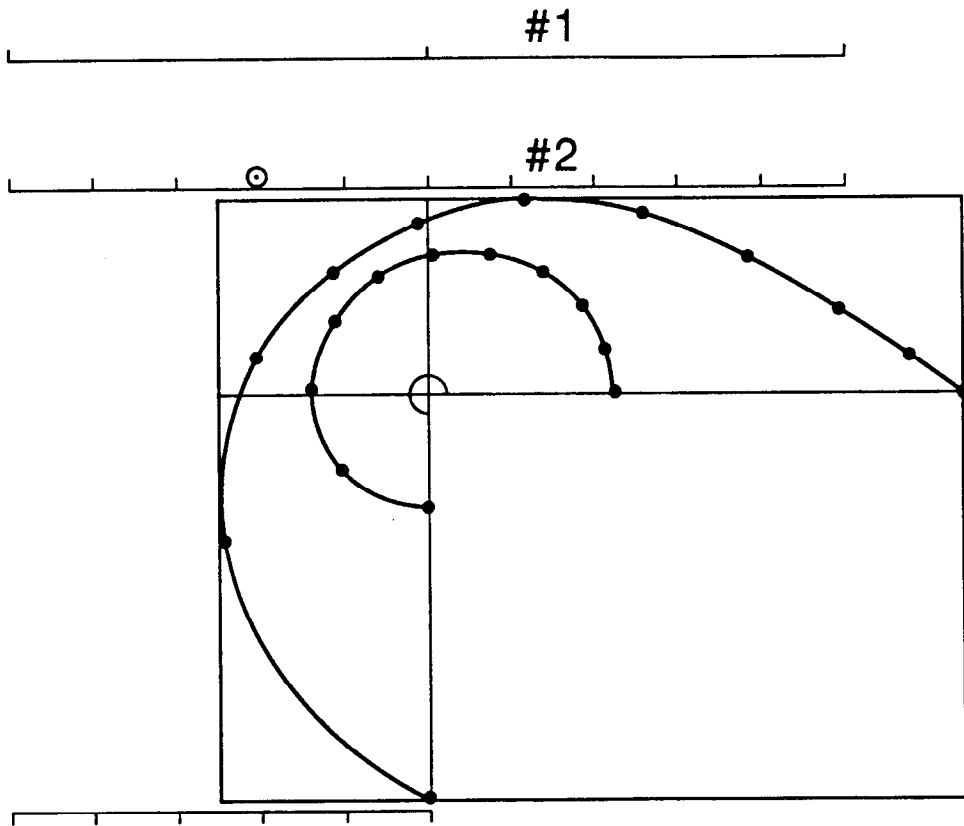
Fig. 15



9-89

6473A16

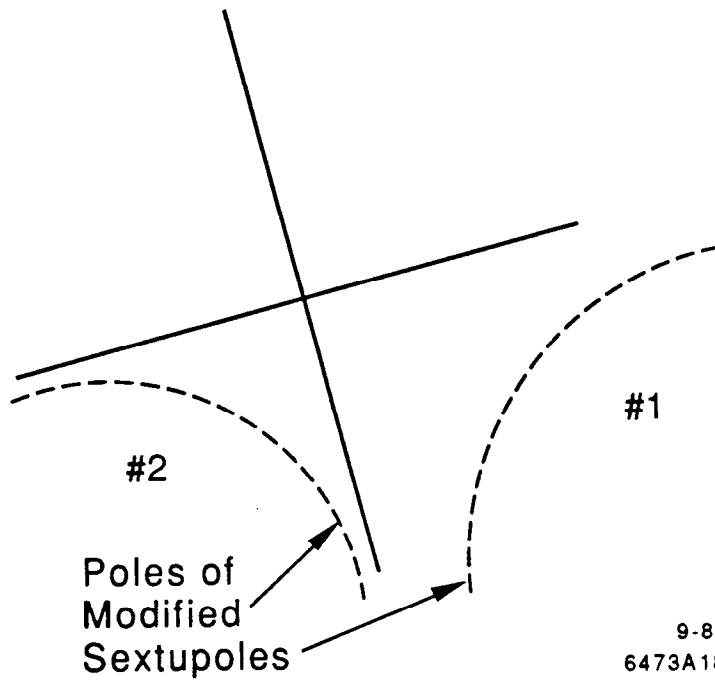
Fig. 16



9-89

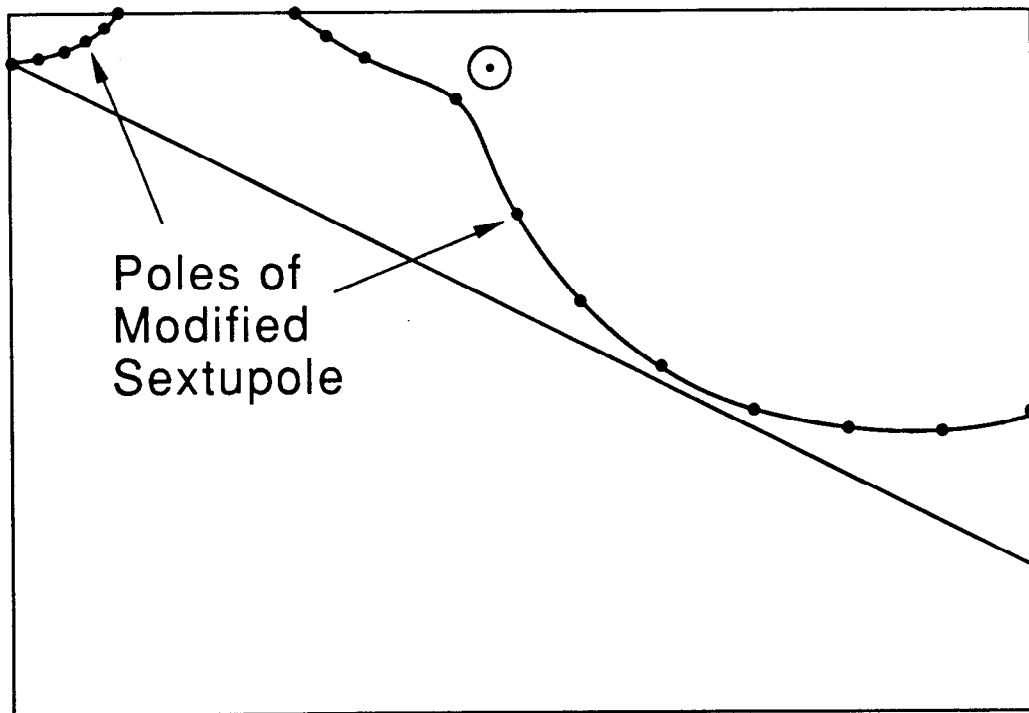
6473A17

Fig.17



9-89
6473A18

Fig. 18



9-89

6473A19

Fig. 19